Zuzanna Szymańska · Jakub Urbański · Anna Marciniak-Czochra

Mathematical modelling of the influence of heat shock proteins on cancer invasion of tissue

Received: date / Revised: date

Abstract Tumour cell invasion is crucial for cancer metastasis, which is the main cause of cancer mortality. An important group of proteins involved in cancer invasion are the Heat Shock Proteins (HSPs). According to experimental data, inhibition of one of these proteins, Hsp90, slows down cancer cells while they are invading tissue, but does not affect the synthesis of matrix metalloproteinases (MMP2 and MMP9), which are very important for cancer metastasis, acting as extracellular matrix (ECM) degrading enzymes. To test different biological hypotheses regarding how precisely Hsp90 influences tumour invasion, in this paper we use a model of solid tumour growth which accounts for the interactions between Hsp90 dynamics and the migration of cancer cells and, alternatively, between Hsp90 dynamics and the synthesis of matrix degrading enzymes (MDEs). The model consists of a system of reaction-diffusion-taxis partial differential equations describing interactions between cancer cells, MDE, and the host tissue (ECM). Using numerical simulations we investigate the effects of the administration of Hsp90 inhibitors on the dynamics of tumour invasion. Alternative mechanisms of reduction of cancer invasiveness result in different simulated patterns of the invading tumour cells. Therefore, predictions of the model suggest experi-

Zuzanna Szymańska
ICM, University of Warsaw, Pawińskiego 5a, 02-106 Warszawa
Poland
Tel.: +48(22) 554 08 44, Fax: +48(22) 554 08 01, E-mail: mysz@icm.edu.pl

Jakub Urbański
Molecular Biology Department, International Institute of Molecular and Cell Biology ul. Ks. Trojdena 4, 02-109 Warsaw,
Poland

Anna Marciniak-Czochra
Center for Modeling and Simulations in the Biosciences (BIOMS), IWR, University of Heidelberg, Im Neuenheimer Feld 294, 69120 Heidelberg,
Germany

ments which might be performed to develop a deeper understanding of the tumour invasion process.

Keywords Cancer invasion · Haptotaxis · Heat shock proteins

Mathematics Subject Classification (2000) 35K55 · 35K57 · 35Q80 · 65M20 · 92-08 · 92C17 · 92C50

1 Introduction

Tissue invasion is one of the most important steps in cancer metastasis. However, the precise mechanisms of this process and all the regulatory pathways governing the invasion are not yet completely understood. Developing effective therapeutic approaches to limit the formation of secondary tumours requires not only the identification of matrix degrading enzymes necessary for invasion, but also an understanding of the regulation of this process.

Tumour invasion consists of four main steps: cancer cell adhesion to the extracellular matrix, secretion of the matrix degrading enzymes and extracellular matrix degradation, the movement or migration of the cancer cells and finally their proliferation. The movement of cancer cells through the tissue involves several different mechanisms, including:

- chemotaxis, where a gradient of a diffusible chemical substance (chemoattractant) can direct the migration of cancer cells to spatial regions of high concentration of the chemoattractant;
- haptotaxis, where cells respond to gradients of non-diffusible chemicals and migrate towards their higher concentrations, i.e. components of the extracellular matrix such as fibronectin, vitronectin, laminin, collagen;
- convection, where cells are passively transported by a deforming substratum;
- random motility or dispersal, where cells respond to local variations in the cell density and tend to move down the density gradient in no preferred direction [21].

All types of movement are conditioned by the motility of the cells (which depends mainly on their ability to reorganise their cytoskeleton) and, to some extent, by their ability to degrade the extracellular matrix. Active migration of cancer cells through the extracellular matrix (ECM) is possible due to the breakdown of ECM components. This process is catalyzed by numerous proteolytic enzymes secreted by the invading cancer cells. Generally, the cancer cells secrete the enzymes which may diffuse into the ECM and degrade one or more of the ECM constitutive proteins e.g. collagen, fibronectin, vitronectin, laminin. Through a combination of proliferation and migration the cancer cells then invade and spread into the ECM. Most of these proteases belong to two general classes: metalloproteases (MMPs) [24] and serine proteases, such as urokinase plasminogen activators (uPAs) [3].

There is a growing evidence to suggest that Heat Shock Proteins (HSPs) play an important role in cancer invasion. An elevated level of two such proteins - Hsp70 and Hsp90 - has been reported in many tumours [16]. Upregulated expression of these proteins observed in tumours raises intriguing

questions as to whether the HSPs contribute to the process of tumourigenesis and cancer cell proliferation [15].

Heat shock proteins are encoded by genes, whose expression is elevated while the cells are subjected to stress conditions, such as heat shock, oxidative stress, fever or inflammation the presence of alcohol, inhibitors of energy metabolism, heavy metals [34]. Under stress conditions HSPs increase cell survival, protecting and disaggregating stress-labile proteins [32], as well as promoting the proteolysis of the damaged proteins [33]. Most of the heat shock proteins can be referred to as "molecular chaperones" that assist the correct non-covalent assembly of other polypeptide-containing structures but which are not components of this assembled structure when they are performing their normal biological function. They bind to unfolded proteins as well as to denaturated proteins promoting their proper folding or refolding or targeting misfolde proteins towards degradation.

Under normal conditions, HSPs have multiple "housekeeping functions" in cells. Their main function is folding new or distorted proteins into their proper shape (which is essential for their activity and function). HSPs, amongst them both alpha and beta isoforms of Hsp90, that make up to 3 % of the total cell soluble proteins, are directly or indirectly involved in many important processes such as protein and vesicular transport, cytoskeleton remodelling, signal transduction, sorting proteins towards degradation and antigen presentation. Many of the important signalling cascades are dependent to some extent on Hsp90 activity. Hsp90 also mediates the activity of transcription factors, such as the p53 protein (well known as a tumour suppressor) or HSF1 (heat-shock factor), a crucial element of the stress response pathway. Hsp90 has also been described as a chaperone for the many proteins commonly linked to cancer progression, such as matrix degrading enzymes, a very important group of proteases involved in the degradation of the ECM (extracellular matrix).

Previously several studies have incorporated mathematical models for cancer invasion and metastasis, for example, Refs. [1,2,5,7,8,12,22,23]. Many of these papers examine the spread of cancer cells using systems of partial differential equations where the cancer cell migration is governed by random motility, i.e. diffusion, and the directed response of the cells to extracellular matrix (ECM) gradients, i.e. haptotaxis. The ECM gradients are created when the ECM is degraded by the matrix degrading enzymes (MDEs) secreted by the cancer cells.

In contrast, the literature concerning the mathematical modelling of heat shock proteins is rather limited. Previous mathematical models of heat shock proteins include those of Peper *et al.* [25] and Rieger *et al.* [26,27]. All these papers examine the changes in Hsp70 synthesis in response to external stimuli such as heat. However, until now there are no mathematical models investigating the impact of heat shock proteins on tumour invasion.

In this paper we extend a generic solid tumour invasion model to test different biological hypotheses on how Hsp90 influences tumour invasion, and in particular, on the possible mechanisms of the reduction of invasiveness due to the administration of Hsp90 inhibitors. Results of the simulations of our models indicate possible directions of further experimental investigations.

The mathematical model considered here involve solid tumour growth in its initial, avascular stage, and is focused on the interactions between the cancer cells and the surrounding tissue. Initially (see Sect. 2), we consider a mathematical model consisting of three partial differential equations (PDEs), which describes the evolution in time and space of the cancer cell density (denoted by u), the extracellular matrix protein density (denoted by v) and the matrix degrading enzyme concentration (denoted by m). Further on, (see Sect. 3) we extend the generic model, focusing on the specific role of Hsp90. Using our mathematical model, we consider two hypotheses that can explain the phenomenon of attenuated invasiveness upon administration of Hsp90 inhibitors. First, that Hsp90 influences the activation/production of enzymes degrading the extracellular matrix (not necessarily MMP2), and second, that Hsp90 affects the cell cytoskeleton and increases a cell's "flexibility" and, therefore, its invasiveness. To validate our models we performed experiments examining the relationship between Hsp90 dynamics and malignant cell motility. Outcomes of the *in vitro* experiments are presented in Section 4, while their comparison to the predictions of our model are presented in the final section (see Sect. 5).

2 The basic mathematical model

We now describe the way in which the cancer cell density $u(x,t)$, the extracellular matrix density $v(x,t)$ and matrix degrading enzyme concentration $m(x,t)$ are involved in invasion. Subsequently, we present partial differential equations of the spatio-temporal evolution of each variable.

(a) ***Cancer Cells:***

The two key factors governing cancer cell migration during invasion are random motion and haptotaxis (in response to gradients of fibronectin, vitronectin and other ECM components). In addition to migration, the model includes a term modelling cancer cell proliferation in the form of a logistic growth law accounting for the competition for space.

The equation describing the dynamics of the cancer cells is given by:

$$\frac{\partial u}{\partial t} = \underbrace{\nabla \cdot (D_u(u,v)\nabla u)}_{\text{random motility}} - \underbrace{\nabla \cdot (\chi_u(v)u\nabla v)}_{\text{haptotaxis}} + \underbrace{F(u,v),}_{\text{proliferation}} \tag{1}$$

where $F(u,v) = \mu_u u(1-u-v)$, and $\mu_u > 0$.

In general, the random motility of the cancer cells may depend on the density of the cancer cells themselves and the concentration of the ECM. In such a case it should be modelled using a function $D_u(u,v)$ depending on the variables u and v. However, for simplicity, in this model we do not consider such a dependency. In our basic model (and later in our model with Hsp90 dependent MDE activation) $D_u(u,v)$ is taken to be a constant and equal to D_u.

In a similar manner to the cell random motility, the haptotaxis function

may depend on the concentration of ECM (see, for example, [29]). However, again, for simplicity, we omit this dependency and in our basic model (as well as in our model with Hsp90 dependent MDE activation) we assume a constant haptotaxis sensitivity function i.e. $\chi_u(v) = \chi_u$.

(b) ***Extracellular Matrix***

It is known that ECM does not diffuse and, therefore, we omit any diffusion term (or other "migration" terms). We model ECM degradation by assuming that the MDEs degrade the ECM upon contact at some (degradation) rate δ_v. We assume that no remodelling of the ECM takes place. The equation for ECM takes the form:

$$\frac{\partial v}{\partial t} = - \underbrace{\delta_v m v.}_{\text{degradation}} \tag{2}$$

(c) ***Matrix Degrading Enzymes***

The spatio-temporal evolution of the concentration of the MDE is assumed to occur through diffusion, production which depends on interaction between the cancer cells and the ECM and loss through simple degradation. The equation for MDE concentration is therefore given by:

$$\frac{\partial m}{\partial t} = \underbrace{D_m \Delta m}_{\text{diffusion}} - \underbrace{\delta_m m}_{\text{degradation}} + \underbrace{H(u,v).}_{\text{production}} \tag{3}$$

Assuming that the MDE production is triggered by the contact between cancer cells and ECM, we take $H(u,v) = \mu_m uv$.
The equations are considered on some domain $\Omega \subset \mathbb{R}^2$ with smooth boundary $\partial\Omega$. Zero flux boundary conditions are imposed along with suitable initial conditions to close the system.

2.1 Non-dimensionalization

We recast the problem in terms of dimensionless variables, rescaling distance with the maximum distance that cancer cells may achieve at the early stage of invasion, i.e. $L = 0.1$ cm and time with $T = \frac{L^2}{D}$, where D represents a reference diffusion coefficient of the enzyme $\sim 10^{-6}$ cm^{2}s^{-1}. Additionally, we rescale densities of cancer cell, ECM and MDE with appropriate reference densities u_0, v_0 and m_0, respectively. Following [13] we assume that the reference densities have nanomolar values. The rescaled variables are:

$$\tilde{t} := \frac{t}{T}, \quad \tilde{x} := \frac{x}{L}, \quad \tilde{u} := \frac{u}{u_0}, \quad \tilde{v} := \frac{v}{v_0}, \quad \tilde{m} := \frac{m}{m_0}.$$

This introduces non-dimensional parameters

$$\tilde{\mu}_u = \tau\mu_u, \quad \tilde{\mu}_m = \tau\mu_m, \quad \tilde{\delta}_m = \tau\delta_m, \quad \tilde{\delta}_v = \tau m_0 v_0 \delta_v,$$

$$\tilde{D}_u = \frac{D_u}{D}, \quad \tilde{D}_m = \frac{D_m}{D}, \quad \tilde{\chi}_u = \frac{\chi_u}{D}.$$

After a subsequent nondimensionalization of the parameters in the functions F, H, and dropping tildes for notational convenience, we obtain the nondimensional system of equations,

$$\begin{cases} \dfrac{\partial u}{\partial t} = D_u \Delta u - \chi_u \nabla \cdot (u \nabla v) + \mu_u u(1-u-v), \\ \dfrac{\partial v}{\partial t} = -\delta_v m v, \\ \dfrac{\partial m}{\partial t} = D_m \Delta m - \delta_m m + \mu_m u v. \end{cases} \tag{4}$$

2.2 Parameter estimation

Before we carry out computational simulations of our model with appropriate initial conditions and zero flux boundary conditions, we need to estimate at least those parameters which can be found elsewhere in the literature or on the basis of performed experiments.

Estimation of the Diffusion Coefficients D_u and D_m

As has been mentioned previously, we introduce D, a reference chemical diffusion coefficient *e.g.* $D \sim 10^{-6} cm^2 s^{-1}$ [4]. Estimates for the cell random motility coefficient vary depending on the cell type: $3 \times 10^{-9} cm^2 s^{-1}$ - $5.9 \times 10^{-11} cm^2 s^{-1}$ for epidermal cells [28]; $(7.1 \pm 2.7) \times 10^{-9} cm^2 s^{-1}$ for endothelial cells [31]. In light of these data, our choice for the cell random motility coefficient D_u will vary betweeen $10^{-9} cm^2 s^{-1}$ and $10^{-11} cm^2 s^{-1}$, and so our nondimensional value will be between $10^{-3} - 10^{-5}$. Following Gerisch and Chaplain [**?**] we assume an estimate for $u_0 = 6.7x10^7$ cell cm^{-3}.

Assuming that the diffusion coefficient of a diffusible chemical is in the range 10^{-9}-10^{-6}cm^{2}s^{-1} (see [6,28]) we obtain a dimensionless estimate of D_m in the range 0.001 - 1. We leave the reference MDE concentration m_0 unspecified due to difficulties in obtaining suitable experimental values (cf. [**?**]).

The haptotactic coefficient χ_u

Stokes *et al.* [31] estimated the chemotactic sensitivity of ECs migrating in a culture containing αFGF, to be $2600 cm^2 s^{-1} M^{-1}$ (see [31]). In the absence of reliable empirical data, we chose the haptotaxis sensitivity χ to be in the range of $2.5 \times 10^{-3} - 2.5 \times 10^{-1}\, cm^2 s^{-1} M^{-1}$. Therefore, considering the fact that the vitronectin blood plasma concentration is around $4\mu M$ [9], leads to a dimensionless estimate of the haptotaxis coefficient χ_u in the range between 0.001 - 1. A value of v_0 in the range $0.38 \times 10^{-9} M - 0.38 \times 10^{-12} M$ is consistent with experimental measurements.

Proliferation rate constant, $\mu_{\mathbf{u}}$

Using our in vitro experimental observations we can estimate the proliferation rate (data not shown). On average one cell division takes between 8 and 12 hours. This gives the proliferation rate to be in the range of 0.058 and 0.087 h^{-1}, and thus yields the value of the dimensionless parameter μ_u in the range 0.9 - 1.45.

Remaining Parameters

Not all parameters in the model could have been estimated. Therefore, we chose these values in order to give the best qualitative results in the simulations. For the extracellular matrix degradation rate we consider δ_v to vary between 1 and 20, and for the decay of MDE we consider δ_m to vary between 10^{-1} and 10. Considering the MDE secretion from the cancer cells we chose the nondimensional value of μ_m to vary between 0.01 - 5.

Parameter	**Description**	**Value**
D_u	cell diffusion coefficient	10^{-5} - 10^{-3}
D_m	MDE diffusion coefficient	10^{-3} - 10
χ_u	haptotaxis coefficient	10^{-3} - 1
μ_u	proliferation rate of cancer cells	0.9 - 1.45
μ_m	production rate of MDEs	0.01 - 5
δ_v	rate of degradation of ECM	1 - 20
δ_m	decay of MDE	10^{-1} - 10

Table 1: The range of the estimated values of the model parameters.

2.3 Geometry of the problem

For simplicity we recast to one dimension: $x \in [0, L]$, where x denotes the distance from the centre of the tumour.

2.4 Boundary and initial conditions

Boundary conditions: Because our system refers to *in vitro* experimental protocol, where invasion takes place within an isolated system, we assume that there is no-flux of cancer cells and MDE across the boundary of the domain.
Initial conditions: The initial distribution of the tumour cells, the extracellular matrix density and MDEs concentration are prescribed as follows.

Initially we assume that there is a cluster of cancer cells already present and that they have penetrated a short distance into the extracellular matrix while the remaining space is occupied by the matrix alone. Combining the above results in the following initial conditions:

$$u(x,0) = \exp(\frac{-x^2}{\epsilon}),\ x \in [0,L] \text{ and } \epsilon > 0,$$
$$v(x,0) = 1 - \exp(\frac{-x^2}{\epsilon}),\ x \in [0,L] \text{ and } \epsilon > 0,$$
$$m(x,0) = \frac{1}{2}\exp(\frac{-x^2}{\epsilon}),\ x \in [0,L] \text{ and } \epsilon > 0,$$

where $\epsilon = 0.01$.

2.5 Travelling wave solutions

Given the structure of our partial differential equations (reaction-diffusion-taxis), we now examine if the invasion of the tissue by the cancer cells may be represented by travelling wave solutions of the model (4). System (4) has three types of constant steady state solutions:

$$(0,0,0),\ \ (0,v^*,0),\ \ (1,0,0).$$

Here v^* is any positive constant and yields a continuum of steady-state solutions. The first, trivial steady state is not relevant biologically. The second steady state represents healthy tissue in the absence of any cancer cells. The third solution describes the situation when there are only cancer cells. Since we are modelling invasion of the cancer cells, we may expect a travelling wave solution $u(x,t) = U(x-ct)$ with positive speed $c > 0$, so that there we have the healthy steady state ahead of the wave and the cancer-only one behind the wave.

Thus, we solve this model on the infinite x domain $x \in \mathbb{R}$ with (u,v,m) tending to $(1,0,0)$ as $x \to -\infty$ and (u,v,m) tending to $(0,v^*,0)$ as $x \to +\infty$. We look for solutions which have a constant shape and move in a space with constant speed c, i.e.,

$$u(x,t) = U(z),\ v(x,t) = V(z),\ m(x,t) = M(z), \tag{5}$$

with $z = x - ct$. Transforming system (4) into travelling wave coordinates yields the system of five ordinary differential equations,

$$U' = \Phi,$$
$$\Phi' = -\frac{c}{D_u}\Phi + \frac{\chi_u\delta_v}{cD_u}\Phi MV + \frac{\chi_u\delta_v}{cD_u}\Psi UV + \frac{\chi_u\delta_v^2}{c^2D_u}UVM^2 - \frac{\mu_u}{D_u}U(1-U-V),$$
$$V' = \frac{\delta_v}{c}MV,$$
$$M' = \Psi,$$
$$\Psi' = -\frac{c}{D_m}\Psi + \frac{\delta_m}{D_m}M - \frac{\mu_m}{D_m}UV,$$

where $\Phi(z) = dU/dz$ and $\Psi(z) = dM/dz$ and c is a the wave speed.
There exist three nonnegative steady states of this system, namely

$$(0,0,0,0,0), \quad (0,0,v^*,0,0), \quad (1,0,0,0,0),$$

where $(1,0,0,0,0)$ refers to the cancer-only steady state and $(0,0,v^*,0,0)$ to the healthy steady state. For the solution connecting the cancer-only and healthy steady states to exist, the state $(1,0,0,0,0)$ must have at least a one-dimensional unstable manifold and $(0,0,v^*,0,0)$ at least a one-dimensional stable manifold. Indeed, linear stability analysis shows that the healthy steady state is linearly unstable, while a cancer-only steady state has a two-dimensional stable manifold.

These stability results suggest that we may expect travelling wave solutions, where the cancer cells invade the healthy tissue, replacing it as they invade. Since a five-dimensional phase space analysis does not provide a productive way for seeking travelling wave solutions, we perform numerical study to examine the wave character of the model solutions (see subsequent Section).

A deeper qualitative understanding of the invading solutions is provided by an analysis of reduced and simplified models. Assuming that matrix degrading enzyme has only a local influence on the tissue, i.e. $D_m = 0$, and its dynamics is seen to be on a shorter time scale than the dynamics of the cancer cells and ECM [17], leads to the reduction of model (4) to

$$\begin{cases} \dfrac{\partial u}{\partial t} = D_u \Delta u - \chi_u \nabla \cdot (u \nabla v) + \mu_u u(1-u-v), \\ \dfrac{\partial v}{\partial t} = -\frac{\delta_v \mu_m}{\delta_m} u v^2. \end{cases} \tag{6}$$

A model of this type (but with a proliferation function $u(1-u)$ not depending on the ECM concentration as we have here) was examined by several authors [17–20]. Travelling wave solutions were observed in the case of pure diffusion, pure haptotaxis and a combination of the two migration mechanisms. It was shown that a pure diffusive migration yields smooth solutions [19], while for pure haptotactic migration, the existence of discontinuous solutions with shocks was also shown [17–19]. For the model with a combination of diffusive and haptotactic migration, smooth solutions were found only numerically [19]. It was shown that the minimum wave speed is proportional to D_u for pure diffusive migration and proportional to χ_u for pure haptotactic migration [19]. For the model with diffusion and haptotaxis, the speed of the travelling wave was investigated only numerically. Numerical studies revealed that the minimum speed of the travelling wave is bounded by

$$max(K\sqrt{\chi_u}, 2\sqrt{D_u}) < c_{min} < \sqrt{4D_u + K^2\chi_u},$$

where K is some function of the parameters of the model kinetics.

To estimate the speed of the advancing front of our nonlinear model with diffusion and haptotaxis, we simplify the model further in order to make it amenable to mathematical analysis. Following [6], we assume a constant

gradient of the extracellular matrix, i.e. $\partial_x v = \kappa$. Under this assumption the model reduces to a single Fisher-type equation describing the dynamics of the cancer cells,

$$\partial_t u = D_u \Delta u - \kappa \chi_u \partial_x u + \nu_u u(1-u), \tag{7}$$

where ν_u is rescaled μ_u. For such a model one may estimate the speed of the invading wave as:

$$\kappa \chi_u + 2\sqrt{D_u \nu_u},$$

where κ is a parameter measuring the gradient of the tissue (see for example [13] or [6]). These results, obtained for the reduced, simplified models, indicate that any mechanism which interferes with and reduces either the haptotaxis parameter χ_u or the random motility coefficient D_u should slow down the rate of invasion of the cancer cells. It gives an indication regarding the relationship between the speed of the invasion of cancer cells and their migration properties.

In the subsequent section we investigate the dynamics of the original model (4) numerically. Our numerical studies show that, although the solutions of the PDE system have much more complicated dynamics and the profiles change in time, in a qualitative maner they reflect the main features of the solutions obtained for the reduced models.

2.6 Simulation Results

In this section we present computational results obtained from numerical simulations of system (4). The systems of equations considered here were solved using the Method of Lines and Gear's Method. The PDEs were discretized in space to give a system of ODEs [30]. The resulting system of ODEs were then solved using Backward Differentiation Formulae e.g. the Backward Euler Method (implicit, multi-step methods for stiff systems), and implemented using the NAG Routine DO3PCF and also the MATLAB PDE solver PDEPE.

The simulations show that the qualitative behaviour of solutions is similar for the whole set of admissible parameters, i.e. parameters estimated in subsection 2.2. Therefore, we present here results obtained for the particular choice of parameters:

$$D_u = 0.00035,\ D_m = 0.00491,\ \chi_u = 0.0285,$$

$$\mu_u = 1,\ \mu_m = 0.5,\ \delta_v = 8.15,\ \delta_m = 0.5.$$

As can be seen from the plots in Fig. 1, the simulated solution of the ECM concentration has the character of a travelling front moving to the right. The solution of the evolution of the cancer cell density shows more complicated dynamics. However, the leading edge of the tumour exhibits also a wave-like behaviour, and an advancing front of cancer cells successfully invades the ECM. The production and secretion of the MDEs is highly regulated. MDE production is localised as is observed experimentally and clinically. MDEs

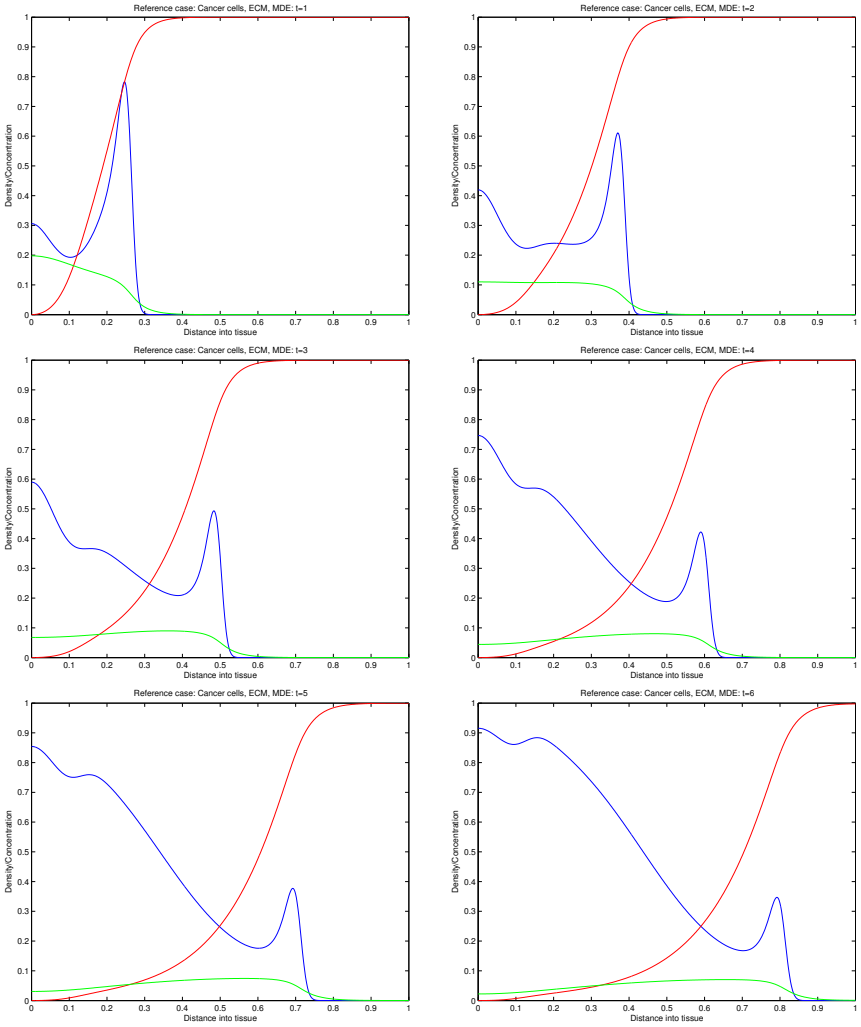

Fig. 1 Plots at times $t = 1, 2, 3, 4, 5, 6$ showing the spatio-temporal evolution of the density of cancer cells (blue) and the concentrations of ECM (red) and MDEs (green). The figures show an invading advancing front of cancer cells producing MDEs which, then, diffuse and degrade the matrix. The cancer cells migrate and proliferate into the empty space of the degraded ECM. Simulations were performed for the set of parameters $D_u = 0.00035$, $D_m = 0.00491$, $\chi_u = 0.0285$, $\mu_u = 1$, $\mu_m = 0.5$, $\delta_v = 8.15$, $\delta_m = 0.5$.

diffuse and degrade the ECM creating empty space into which the migrating and proliferating cancer cells move. The simulations indicate that initially haptotaxis leads to the formation of a sharp peak of cancer cell density on the leading edge of the tumour. Later, proliferation starts to play an important role leading to a maximum in cancer cell density in the centre of solid tumour followed by a second local maximum on the edge of the tumour.

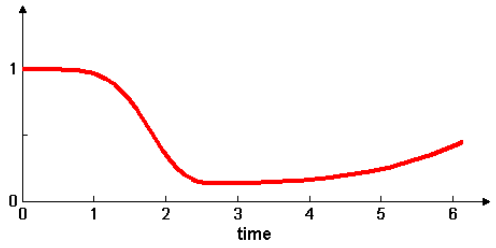

Fig. 2 Plot of the time evolution of the pool of the Hsp90 unbound to the inhibitor after its administration (active Hsp90).

3 Modelling the role of Hsp90

In this section we extend our model (4), to explore the impact of Hsp90 on the invasiveness of the cancer cells. Using a baseline model and combining modelling and simulation with experimental investigations, we check two different hypotheses concerning the impact of Hsp90 on the invasiveness of malignant cells:

(H1) Hsp90 regulates the activation (production) of enzymes degrading the extracellular matrix (not necessarily MMP2) and, thus, reduced active Hsp90 concentration leads to the impaired MDE activation;
(H2) Hsp90 affects the cytoskeleton, both in a direct and indirect way. Directly, interacting with the major cytoskeletal proteins such as actin and tubulin or indirectly via signalling pathways. It is widly known that there is a whole variety of kinases involved in cell signaling amongst Hsp90 client proteins. Influencing cytoskeleton Hsp90 incereases a cell's "flexibility" and, therefore, the decrease in active Hsp90 concentration leads to the reduced cell migration.

We now modify system (4) to model the above two scenarios, and introduce a time-dependent function of active Hsp90 concentration, denoted by $h(t)$. Upon inhibitor binding Hsp90 becomes inactive. We assume that the time evolution of active Hsp90 concentration after admnistration of its inhibitors is known, and given by the curve presented in Fig.2. This corresponds to the experimental observations showing that, after the administration of the inhibitors, active Hsp90 concentration decreases and then slowly rises again to its physiological level. We do not consider the spatial distribution of Hsp90, because the focus of the model is on the processes which are pressumably regulated by Hsp90 inside the cell or on the cell membrane.

3.1 Model with Hsp90 dependent MDE activation

Hypothesis ($H1$) is based on reports which point to Hsp90 as a crucial factor in the activation of the matrix degrading enzyme MMP2 [10]. MMP2

is one of the major proteins involved in ECM degradation. Eustace *et al.* (2004) suggest that Hsp90 directly activates MMP2 and therefore promotes the degradation of extracellular matrix by cancer cells. Active MMP2, secreted to the extracellular space, enables tumour invasion. In the case where the concentration of active Hsp90 is not high enough, a cell loses its ability to secrete enzymes that degrade components of the surrounding tissue and therefore is not able to invade (or at least the invasion is significantly slowed down). To model this hypothesis we modify our function $H(u,v) = \mu_m uv$ and consider

$$H(u,v,h) = \mu_m uvh, \tag{8}$$

where $h(t)$ denotes active Hsp90 concentration in time, given explicitly as the function of time in Fig. 2. It reflects the assumption that the concentration of Hsp90 is homogeneous in respect to space, i.e. the same in every cell, and depends only on time.

3.1.1 Numerical results

In the first modification of model (4), as previously noted, we assume that Hsp90 either directly activates or takes part in producing an active form of MDEs. We assume that active Hsp90 concentration changes over time as shown in Fig. 2. This leads to an insufficient amount of active Hsp90 in the cancer cells and therefore to impaired/reduced MDE production.

Fig. 3 shows the results of the simulations of system (4) with $H(u,v,h)$ given by (8) and h given by the function depicted in Fig. 2. As can be seen in Fig. 3, the first two plots, at time $t = 1, 2$, are similar to the first two plots presented in Fig. 1. We observe an advancing front of cancer cells invading the ECM. However, at later times the speed of invasion slows down due to the reduced MDE production rate and at time $t = 6$ cancer cells have penetrated less deeply into the ECM. In this case, the leading edge of the invading front reaches a depth only of around 0.73, while in simulations of basic model (4) it reaches a depth of around 0.86 (see Fig. 1).

3.2 Model with variable cell flexibility

Hypothesis ($H2$) assumes that Hsp90 is an important factor affecting key biomechanical properties of the cell cytoskeleton, i.e. the cell's "flexibility". In the case where there is a lack of active Hsp90, a cell loses the ability to reorganise its cytoskeleton. This leads to an increase in cell cytoskeleton stiffness, which, in turn, reduces cell random motility and haptotaxis. Therefore, we assume that both the random motility coefficient D_u and the haptotactic coefficient χ_u are functions of Hsp90 concentration and have the following form:

$$D_u(h) = D_u \cdot I(h) \quad \text{and} \quad \chi_u(h) = \chi_u \cdot I(h), \tag{9}$$

where $h(t)$ is a given time-dependent function of active Hsp90 concentration (see Fig. 2), reflecting the administration of Hsp90 inhibitors. The function $I(h)$ describes functional relationship between Hsp90 concentration and the flexibility of a cell.

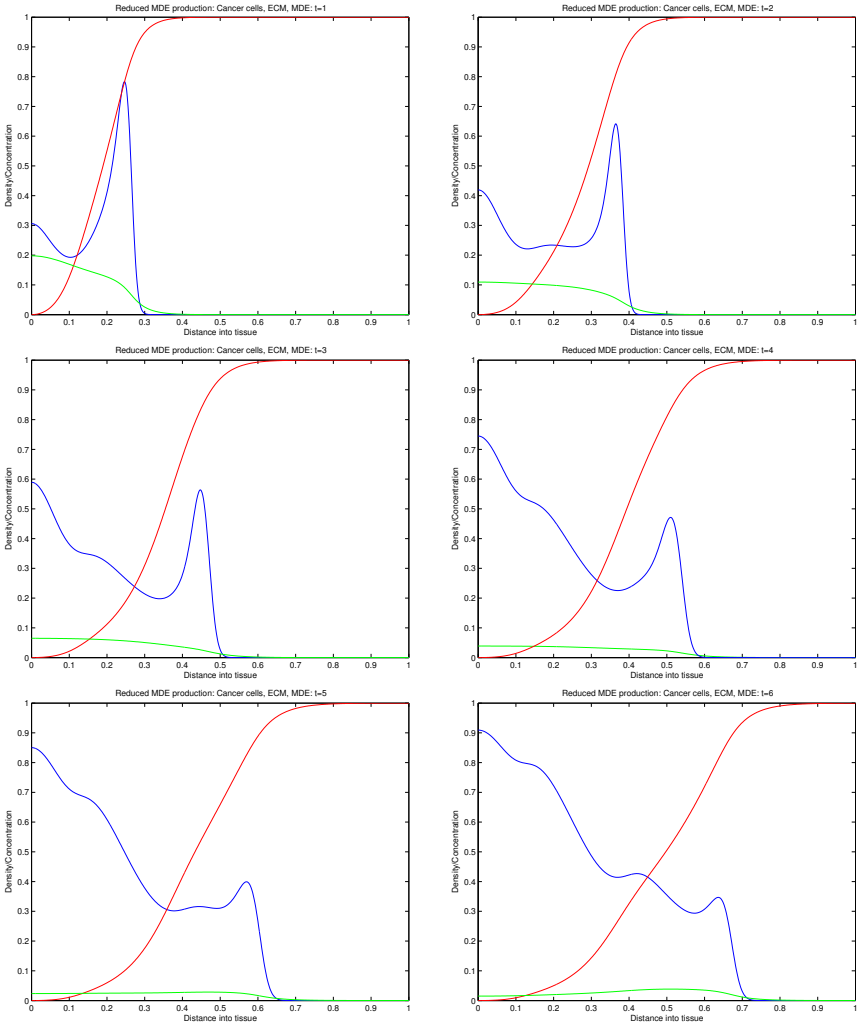

Fig. 3 Plots at times $t = 1, 2, 3, 4, 5, 6$ showing the spatio-temporal evolution of the density of cancer cells (blue), the concentration of ECM (red) and MDEs (green) under the assumption that MDE production rate depends linearly on active Hsp90 concentration (see Eq. 8). Simulations were performed for the parameters as in Fig. 1 and time dependent active Hsp90 concentration $h(t)$ as depicted in Fig. 2.

Since the process of reorganisation of the cytoskeleton involves a number of biochemical reactions, it is distributed in time. Therefore, it seems to be more acurate to assume that the cell's flexibility depends on some distributed time delay functional of Hsp90 concentration rather than on the its concentration in a given time point.

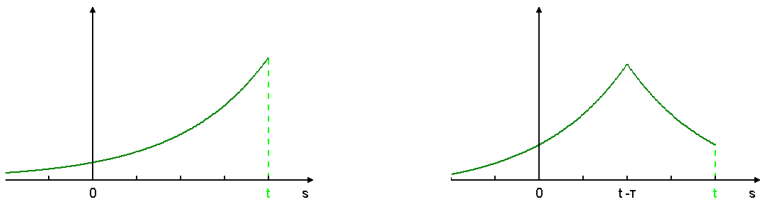

Fig. 4 Plots of the distributed delay kernels $W(t-s) = e^{-(t-s)}$ on the left hand-side and $W(t-s) = e^{-|t-s-\tau|}$ on the right hand-side.

In general, our distributed delay takes the following functional form:

$$I = \int_{-\infty}^{t} W(t-s)h(s)ds, \tag{10}$$

where $W(t-s)$ is the distributed delay kernel, which is a representation of the influence of active Hsp90 concentration in past on the cell's flexibility at the present time point. We consider two cases of the functional $I(h)$ describing the distributed delay, and compare it with the local in time functional $I(h) = h$.

Case 1:

$$W(s-t) = e^{-(s-t)}. \tag{11}$$

This decaying exponential kernel gives weight to all past times, but most weight to "recent" times. Differentiating (10) leads to the following ODE governing the dynamics of I in time:

$$\frac{dI}{dt} = -e^{-t}\int_{-\infty}^{t} e^{s}h(s)ds + e^{-t}[e^{t}h(t)], \tag{12}$$

which is equivalent to

$$\frac{dI}{dt} = -I + h(t). \tag{13}$$

Using (13), we re-write system (4) as:

$$\begin{cases} \dfrac{\partial u}{\partial t} = D_u\nabla\cdot(I\nabla u) - \chi_u\nabla\cdot(Iu\nabla v) + \mu_u u(1-u-v), \\ \dfrac{\partial v}{\partial t} = -\delta_v m v, \\ \dfrac{\partial m}{\partial t} = D_m\Delta m - \delta_m m + \mu_m u, \\ \dfrac{dI}{dt} = -I + h(t). \end{cases} \tag{14}$$

This is a non-autonomous system, since $h(t)$ depends explicitly on time.

Case 2:

$$W(t-s) = e^{-|t-s-\tau|}. \tag{15}$$

This distributed delay kernel gives most weight to events that happened τ time units in the past, i.e. at time $t-\tau$. Applying (15) to (10) results in

$$I = e^{-t}\int_{-\infty}^{t-\tau} e^{s+\tau}h(s)ds + e^{t}\int_{t-\tau}^{t} e^{-s-\tau}h(s)ds. \tag{16}$$

Differentiating (16) leads, after subsequent calculations, to the integro-differential equation describing the temporal dynamics of I:

$$\frac{dI}{dt} = -e^{-t}\int_{-\infty}^{t-\tau} e^{s+\tau}h(s)ds + e^{t}\int_{t-\tau}^{t} e^{-s-\tau}h(s)ds + e^{-\tau}h(t).$$

Differentiating again yields the equation:

$$\frac{d^2I}{dt^2} = I + e^{-\tau}\Big[h(t) + h'(t)\Big] - 2h(t-\tau). \tag{17}$$

Re-writing the above 2nd order ODE as a system of two 1st order ODEs yields:

$$\begin{cases} \dfrac{dI}{dt} = J, \\ \dfrac{dJ}{dt} = I + e^{-\tau}\big(h(t) + h'(t)\big) - 2h(t-\tau). \end{cases} \tag{18}$$

Again, applying (18) we can replace (4) by the following system of PDEs with delay:

$$\begin{cases} \dfrac{\partial u}{\partial t} = D_u\nabla\cdot(I\nabla u) - \chi_u\nabla\cdot(Iu\nabla v) + \mu_u u(1-u-v), \\ \dfrac{\partial v}{\partial t} = -\delta_v m v, \\ \dfrac{\partial m}{\partial t} = D_m\Delta m - \delta_m m + \mu_m u, \\ \dfrac{dI}{dt} = J, \\ \dfrac{dJ}{dt} = I + e^{-\tau}\big(h(t) + h'(t)\big) - 2h(t-\tau). \end{cases} \tag{19}$$

3.2.1 Simulation Results

We perform numerical simulations of system (4) with the diffusion and haptotaxis coefficients given by (9). We assume that the Hsp90 concentration changes in time according to the curve depicted in Fig. 2. We consider different $I(h)$ corresponding to three cases. In cases 1 and 2 we assume that $I = \int_{-\infty}^{t} W(t-s)h(s)ds$ (see Eq. (10)). In case 1, distributed delay kernel W is given by (11) and in the case 2 distibuted delay is given by (15). In case 3 we assume that I is local in time and given by $I(h) = h(t)$.

Simulations of model (4) under the assumption that a cell's flexibility changes according to Eq. (10), where distributed delay kernel is given by (11) (case 1) are presented in Fig. 5, while the results for the distributed delay kernel given by (15) (case 2) are presented in Fig. 6. Fig. 7 shows the results of numerical simulations performed for $I(h) = h(t)$ (case 3). Figs. 5 and 6 show a very similar advancing front of cancer cells invading the ECM. We note that the speed of invasion slows down very significantly and at time $t = 6$ the cancer cells have penetrated less deeply into the ECM than in the basic model (4) with the constant diffusion and haptotaxis coefficients. The leading edge of the invading front reaches a depth of around 0.55, which is much smaller compared to a depth of penetration of around 0.86 in Fig. 1. Small differences between Figs. 5 and 6 suggest that our system is insensitive to the parameter τ.

In Fig. 7 the advancing front of cancer cells invading the ECM at time $t = 6$ reaches a depth of around 0.61 compared with a depth of around 0.86 in Fig. 1. This is also less than the reduced penetration depth due to lower MDE production shown in Fig. 3. This result may indicate that impairing/reducing haptotaxis is a more effective way to stop cancer invasion than impairing/reducing MDE production.

3.3 Comparison of the models

A comparison of all the results of the numerical simulations of our cancer invasion model (4) and its modifications accounting for the possible interactions between the active Hsp90 concentration in cells and MDE activation and migratory properties of cancer cells is presented in Fig. 8. As mentioned already, we observe significant differences between the speed of the leading edge of the invading tumour in the basic model of the tumour invasion and in the models with the motility coefficients dependent on the level of active Hsp90 and, therefore, reduced after the administration of Hsp90 inhibitors. Moreover, the behaviour of the model solutions does not depend significantly on the particular choice of the functional $I(h)$ describing the dependence of diffusion and haptotaxis on the dynamics of active Hsp90. However, the difference in the range of invasion between the model with the MDE activity depending on Hsp90 and the model with migratory properties controled by Hsp90 dynamics is already significant. The dynamics of the model with Hsp90 dependent MDE activity, (9), resembles more the dynamics of the basic model. This observation suggests that reducing cell motility and hap-

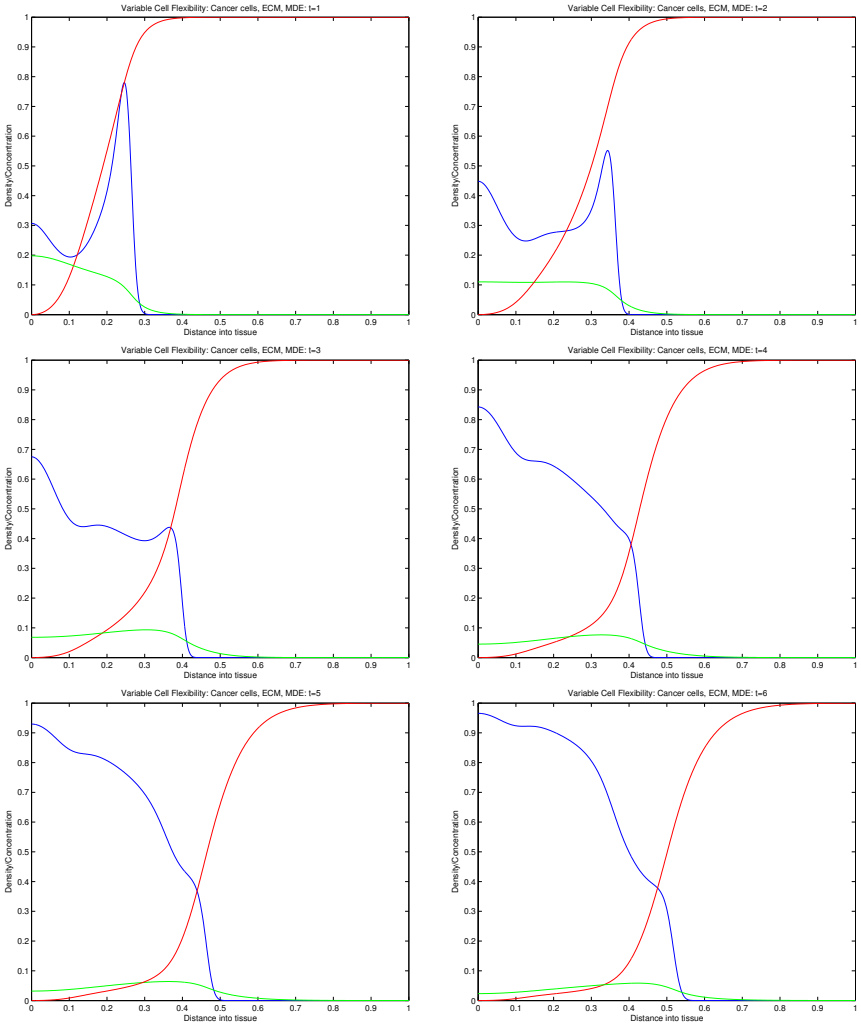

Fig. 5 Plots at times $t = 1, 2, 3, 4, 5, 6$ showing the spatio-temporal evolution of the density of cancer cells (blue) and the concentrations of ECM (red) and MDEs (green) under the assumption that a cell's flexibility depends on active Hsp90 concentration (see Eq. 10), with a distributed delay kernel given by (11). Simulations were performed for the parameters as in Fig. 1 and time dependent active Hsp90 concentration $h(t)$ as depicted in Fig. 2.

totaxis might be a more effective way to slow down cancer invasion than reducing MDE production.

Additionally, we observe different simulated patterns of the invading tumour cells. Numerical solutions of the cell density of the basic model, as well as the model with the Hsp90 dependent MDE activity, exhibit a sharp peak on the edge of advancing front. In the numerical solutions of the model with variable migration coeffcients, such a peak, although it initially also exists,

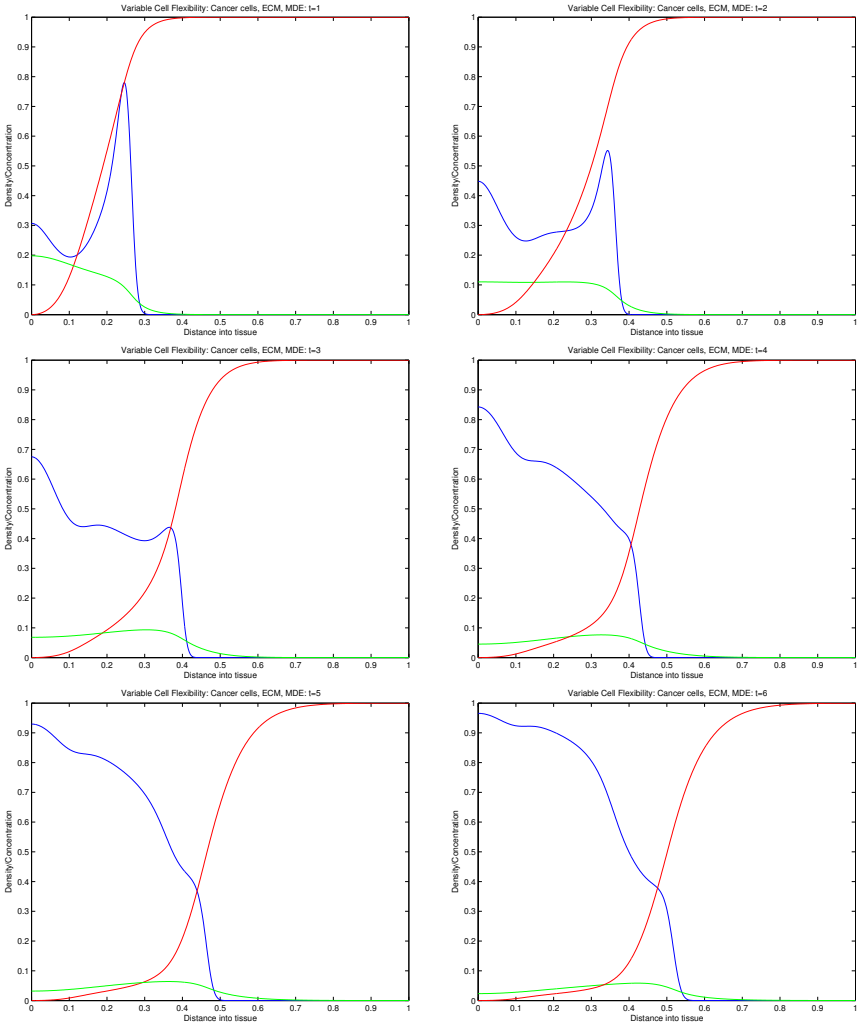

Fig. 6 Plots at times $t = 1, 2, 3, 4, 5, 6$ showing the spatio-temporal evolution of the density of cancer cells (blue) and the concentrations of ECM (red) and MDEs (green) under the assumption that a cell's flexibility depends on active Hsp90 concentration (see Eq. 10), with a distributed delay kernel given by 15. Simulations were performed for the parameters as in Fig. 1 and time dependent active Hsp90 concentration $h(t)$ as depicted in Fig. 2.

disappears by time $t = 3$, and the solution u becomes monotonically decreasing in space. These predictions of the model suggest that experiments investigating the spatial pattern of the tumour cell density might allow one to check which of the hypothetical scenarios of influence of Hsp90 on the cell invasiveness is more plausible.

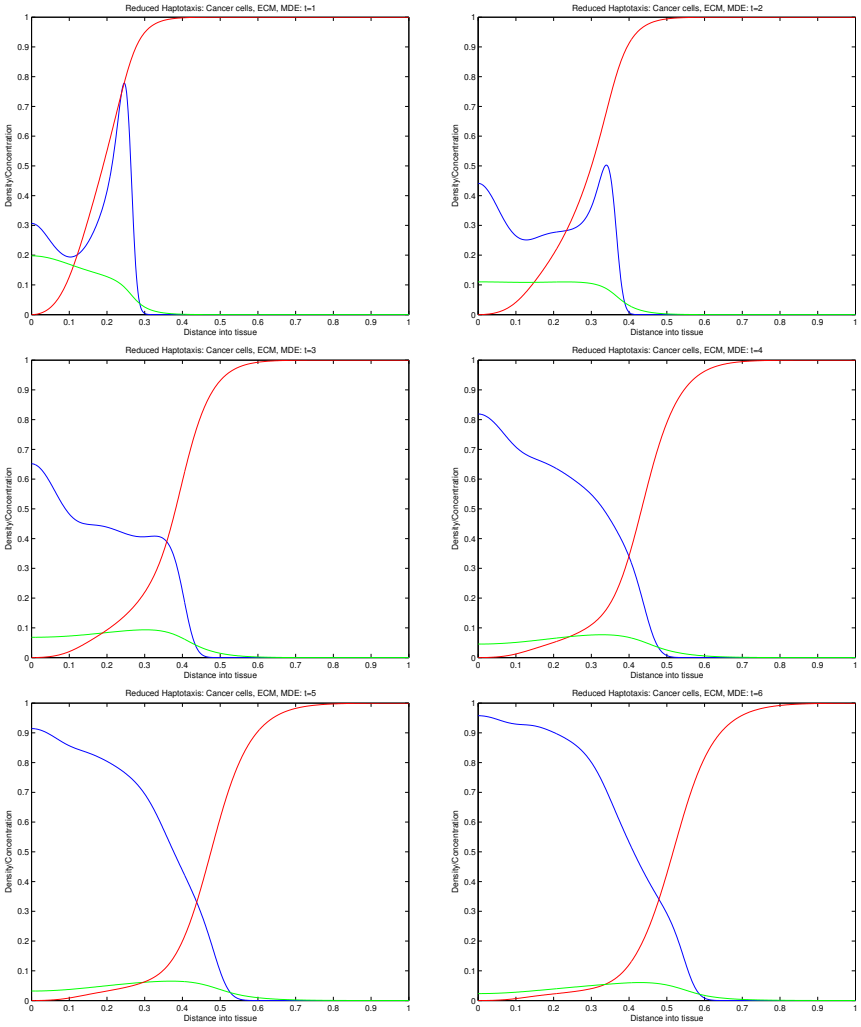

Fig. 7 Plots at times $t = 1, 2, 3, 4, 5, 6$ showing the spatio-temporal evolution of the density of cancer cells (blue) and the concentrations of ECM (red) and MDEs (green) under the assumption that a cell's flexibility depends on active Hsp90 concentration at the current point in time. Simulations were performed for the parameters as in Fig. 1 and time dependent active Hsp90 concentration $h(t)$ as depicted in Fig. 2.

4 In vitro experimental results

To check the hypotheses on the mechanisms of the Hsp90 influence on the cancer invasiveness, we performed certain *in vitro* experiments. Our *in vitro* results show no direct correlation between treatment with 17-(Allylamino)-17-demethoxygeldanamycin and the secretion of active MMP2 and MMP9 gelatinases to the extracellular space (see Fig. 9 and its description for the

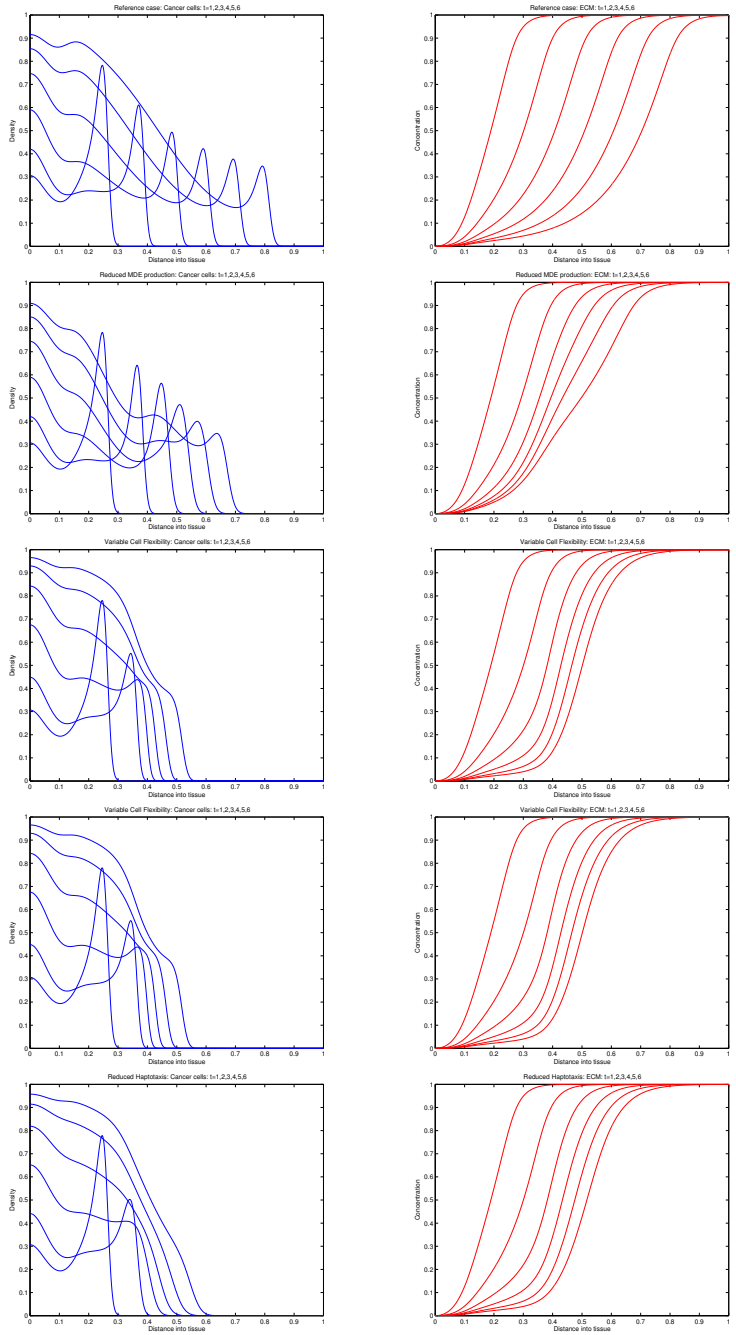

Fig. 8 Plots showing the spatio-temporal evolution of the cancer cells and ECM under the different scenarios considered: baseline (top); reduced MDE production (second); reduced migration - case 1 (third); reduced migration - case 2 (fourth); reduced migration - case 3 (bottom).

technical details of the experiment). Zymographic analysis enables an estimation of active MDE level secreted into the culture medium by the cells. The activity of MMP2 and MMP9, two major MDEs, is compared in figure 9. Activity has been measured in the control medium (lane1) and the medium containing various concentrations of Hsp90 inhibitor (lanes 2 and 3). Our results indicate that Hsp90 inhibition does not have any significant effect on MDE activitity, however, these results not exclude the possibility that decreased activity of MDE contributes to the lower invasion rate. In order to confirm this hypothesis and validate the mathematical model, further experiments with specific siRNA knockdowns of MMP2, MMP9 and MT-MMP1 are being performed.

Hsp90 inhibitors significantly reduce cancer cell invasion in a Matrigel assay (see Fig. 10 and its description for the technical details of the experiment), and to a lesser extent, but still significantly reduce cell motility in a scratch assay (see Fig. 11 and its description for the technical details of the experiment). The Matrigel assay simulates in vivo conditions - cells have to migrate through Matrigel (i.e. ECM isolated from mice) towards higher concentration of the serum. If the cell motility or ECM degrading enzymes activity is impaired, fewer cells migrate to the membrane below the Matrigel layer in a given time. It is a standard method of assaying cell invasion. The Scratch assay is an experimental procedure that enables one to estimate the migration speed of cells. Cells are removed from a part of the culture plate, and the time taken to overgrow the gap is measured. This experiment is performed on plastic plates, and the cells migrate on the plastic instead of ECM. In this experimental system the process of migration is independent of any particular MDE. The results strongly support the hypothesis that the MDE activity is not the only factor that influences cell migration. Collectively these data suggest that the role of Hsp90 in cancer cell invasion is linked to the mediation of the cell motility rather than control of MDE activation and secretion. Since Hsp90 has been reported to interact with components of the cell cytoskeleton, decreased invasion upon geldanamycin treatment might be linked to the cytoskeletal changes.

These results, supported by preliminary *in vitro* experiments on cancer cells strongly suggest that detailed studies on the role and involvement of Hsp90 in cell motility should be performed.

5 Discussion

In this paper we have presented different versions of a mathematical model of cancer cell invasion of tissue. Our models differ from previous models of cancer cell invasion in that they include for the first time the effects of heat shock proteins. We checked a number of hypotheses concerning the impact of Hsp90 on the invasiveness of malignant cells and performed new experiments examining the relationship between Hsp90 dynamics and malignant cell motility.

Our basic mathematical model consists of a system of three coupled nonlinear reaction-diffusion-taxis partial differential equations describing the spatio-temporal evolution of the cancer cell density, the ECM concentration

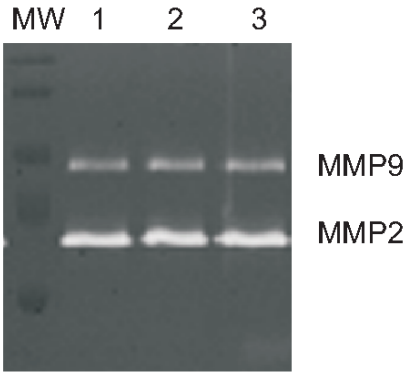

Fig. 9 Zymographic analysis of conditioned cell culture media of MDA-MB 231 breast cancer cells. Cell were grown on IMDM medium with 10% FBS. At the 80% of confluence medium was replaced with serum-free medium supplemented with (1) DMSO - control (2) 0.5 μM 17-AAG (17-(Allylamino)-17-demethoxygeldanamycin) and (3) 1.0 μM 17-AAG. Serum is removed prior to the experiment as it contains MDE and might influence the final result. Upon 24h media were collected and subjected to the zymographic analysis on 10% poliacrylamide gel with 0.1 gelatin.

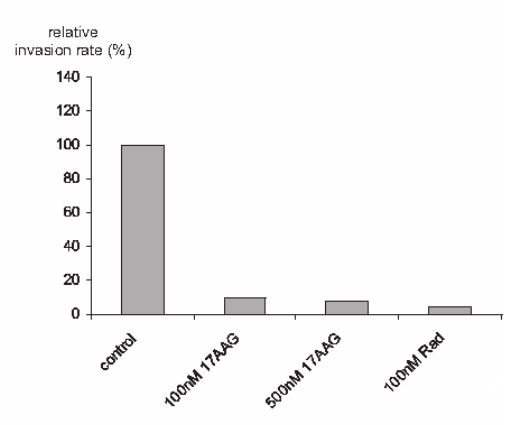

Fig. 10 Relative invasion rate of MDA-MB 231 breast cancer cells in Matrigel assay. In each experiment 25000 cells were plated in upper chamber of Transwell (Costar) insert over the Matrigel layer. Cells suspended in serum free IMDM medium were treated with various concentrations of Hsp90 inhibitors. The lower chamber was filled with IMDM medium with 10% FBS. Aftee 24h of incubation cells bound to the lower surface of the membrane were counted. Relative invasion rate has been assessed (as compared to the control cells).

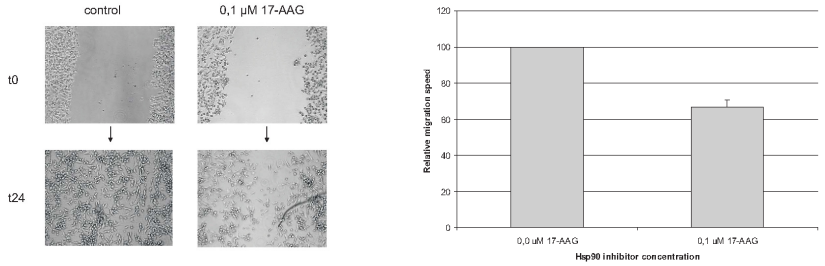

Fig. 11 Migration of MDA-MB 231 breast cancer cells in scratch assay. Cells were grown on IMDM medium with 10% FBS in 24-well plates. At the 80% of confluence medium was replaced with serum-free medium supplemented with (1)DMSO - control or 0,1 μM 17-AAG (17-(Allylamino)-17-demethoxygeldanamycin). Cells were scratched with a pipette tip. Area of scratch has been measured at timepoints of 0h and 24h (A) in triplicate. Relative migration speed - average rate between scratch areas at t24 and t0 has been assessed (B).

and the MDE concentration. Computational simulations of our basic model reveal advancing fronts of cancer cells invading the ECM through proliferation and migration driven by random motility and haptotaxis. Degradation of the ECM is achieved by a controlled production and secretion of MDEs.

To test different hypotheses on how the dynamics of Hsp90 influences tumour invasion, we modified the basic model and included possible interactions between Hsp90, the rate of MDE production and the migratory properties of the cancer cells. We considered two different mechanisms: (i) the impact of Hsp90 on the MDE production, whereby reduced levels of active Hsp90 led to a reduced MDE production rate; (ii) the influence on cell biomechanical properties and hence cell migration, whereby reduced levels of active Hsp90 led to a lower value of the haptotaxis coefficient.

In both cases, inhibition of Hsp90 led to a decrease of the speed of the invasive wave of cancer cells and also to a smaller depth of penetration of the ECM by the cancer cells. Although both mechanisms had similar qualitative effects, our simulations indicated that the reduction in diffusion and haptotaxis had a greater effect on reducing invasion than the reduction of the MDE production rate. Additionally, alternative mechanisms of reduction of invasiveness result in different simulated patterns of the invading tumour cells. Therefore, the predictions of the model suggest experiments which might be performed to check, which of the hypothetical scenarios of interaction is more plausible.

The models were built in a close connection to experimental data. The paradigm was to use the experimental data to build models, and to use the modelling to plan further experiments, rather than explain what is known already. To validate the models, *in vitro* experiments were performed. Our experimental results indicate that inhibition of Hsp90 reduces cell invasiveness, although, contratry to the hypothesis postulated in [10], it does not affect directly the synthesis of metalloproteases (MMP2). The experiments suggest that the role of Hsp90 in cancer cell invasion is connected with the

mediation of the cell motility rather than the regulation of MDE activation and secretion.

The results of mathematical modelling and simulations, supported by preliminary *in vitro* experiments on cancer cells strongly suggest that detailed studies on Hsp90 impact on cells motility should be performed, both experimentally and theoretically using methods of mathematical modelling, analysis and simulations. Signalling pathways are important targets for clinical and therapeutic intervention. Therefore, accurate quantitative and predictive mathematical models of cell transformation and cancer invasion are important for control of tumour growth. Future work will consider making the haptotaxis function depend on key intracellular variables such as HSP concentration. This means adopting a systems biology approach to cancer invasion modelling.

Acknowledgements The authors would like to thank prof. Maciej Żylicz from IIMCB and prof. Willi Jäger from IWR University of Heidelberg for many valuable discussions. This work was supported by a grant from The Ministry of Education and Science, PBZ-KBN 107/P04/2004. The work of ZS was supported by the Polish-German Graduate College: "Complex Processes: Modelling, Simulation and Optimization" and the EU project "Modeling, Mathematical Methods and Computer Simulations of Tumour Growth and Therapy" — M3CSTuTh — Contract No. MRTN–CT–2004–503661 and the Polish SPUB–M Grant. AMC was supported by Center for Modeling and Simulation in the Biosciences (BIOMS) in Heidelberg.

References

1. Anderson A. R. A., Chaplain M. A. J., Newman E. L., Steele R. J. C. and Thompson A. M.: Mathematical modelling of tumour invasion and metastasis. J. Theor. Med. **2** 129 – 154 (2000)
2. Anderson A. R. A., A hybrid mathematical model of solid tumour invasion: The importance of cell adhesion. Math. Med. Biol. **22** 163 – 186 (2005)
3. Andreasen P. A., Kjøller L., Christensen L. and Duffy M. J.: The urokinase-type plasminogen activator system in cancer metastasis: A review. Int. J. Cancer **72** 1 – 22 (1997)
4. Bray D.: Cell Movements: From Molecules to Motility, Garland Publishing, New York-Oxford (2000).
5. Byrne H. M., Chaplain M. A. J., Pettet G. J. and McElwain D. L. S.: A mathematical model of trophoblast invasion. J. Theor. Med. **1** 275 – 286 (1998)
6. Chaplain M.A.J., Giles S.M., Sleeman B.D. and Jarvis R.J.: A mathematical analysis of a model for tumour angiogenesis, J. Math. Biol. **33**, 744–770 (1995).
7. Chaplain M. A. J. and Lolas G.: Mathematical modelling of cancer cell invasion of tissue: The role of the urokinase plasminogen activation system. Math. Mod. Meth. Appl. Sci. **15** 1685 – 1734 (2005)
8. Chaplain M. A. J. and Lolas G., Mathematical modelling of cancer invasion of tissue: Dynamic heterogeneity, Net. Hetero. Med. **1** 399 – 439 (2006)
9. Comper W. D., Extracellular Matrix Volume 2 Molecular Components and Interactions. Hartwood Academic (1996).
10. Eustace B. K., Sakurai T., Stewart J. K., Yimlamai D., Unger C., Zehetmeier C., Lain B., Torella C., Henning S. W., Beste G., Scroggins B. T., Neckers L., Ilag L. L., Jay D. G.: Functional proteomic screens reveal an essential extracellular role for hsp90 alpha in cancer cell invasiveness. Nat. Cell Biol. **6** 507–514 (2004)
11. Eustace B. K. and Jay D. G. Extracellular roles for the molecular chaperone, hsp90. Cell Cycle **3** 1098 – 1000 (2004)

12. Gatenby R. A. and Gawlinski E. T.: A reaction-diffusion model of cancer invasion. Cancer Res. **56** 5745 – 5753 (1996)
13. Gerisch A. and Chaplain M. A. J.: Robust numerical methods for taxis-diffusion-reaction systems: Applications to biomedical problems. Math. Comput. Modelling, **43** 49-75 (2006)
14. Gerisch, A. and Chaplain, M.A.J.: Mathematical modelling of cancer cell invasion of tissue: Local and non-local models and the effect of adhesion. J. Theor. Biol. **250**, 684-704 (2008)
15. Helmbrecht K., Zeise E., Rensing L.: Chaperones in cell cycle regulation and mitogenic signal transduction: a review. Cell Prolif. **6** 341 – 65 2000
16. Jolly C. and Morimoto R. I.: Role of the heat shock response and molecular chaperones in oncogenesis and cell death. J. Natl. Cancer Inst. **92** 1564 – 1572 (2000)
17. Marchant B.P., Norbury J. and Perumpananii A.J. Travelling shock waves arising in a model of malignant invasion, SIAM J. Appl. Math. **2** 463–476 (2000)
18. Marchant B.P., Norbury J. and Sherratt J.A. Travelling wave solutions to a haptotaxix-dominated model of malignant invasion, Nonlinearity **14** 1653–1671 (2001)
19. Landman K.A., Simpson M.J., SLater J.L. and Newgreen D.F. Diffusive and chemotactic cellular migration: smooth and discontinuous travelling wave solutions, SIAM J. Appl. Math. **4** 1420–1442 (2005).
20. A. J. Perumpanani, J. A. Sherratt, J. Norbury, and H. M. Byrne, A two parameter family of travelling waves with a singular barrier arising from the modelling of extracellular matrix mediated cell invasion, Phys. D **126** 145–159 (1999).
21. Murray, J.D.: Mathematical Biology. Springer-Verlag, Berlin Heidelberg (2003)
22. Lachowicz M.: Micro and meso scales of description corresponding to a model of tissue invasion by solid tumours, Math. Mod. Meth. Appl. Sci. **15** 1667 – 1683 (2005)
23. Orme M. E. and Chaplain M. A. J.: A mathematical model of vascular tumour growth and invasion. Math. Comput. Model. **23** 43 – 60 (1996)
24. Parsons S. L., Watson S. A., Brown P. D., Collins H. M. and Steele R. J. C.: Matrix metalloproteinases. Brit. J. Surg. **84** 160– 166 (1997)
25. Peper A., Grimbergen C. A., Spaan J. A., Souren J. E. and van Wijk R.: A mathematical model of the hsp70 regulation in the cell. Int J Hyperthermia **14** 97-124 (1998)
26. Rieger T. R., Morimoto R. I. and Hatzimanikatis V.: Mathematical Modeling of the Eukaryotic Heat Shock Response: Dynamics of the Hsp70 Promoter. Biophys. J. **88** 1646-1658 (2005)
27. Rieger T. R., Morimoto R. I. and Hatzimanikatis V. Bistability explains threshold phenomena in protein aggregation both in vitro and in vivo. Biophys. J. **90** 886-95 (2006).
28. Sherratt J. A. and Murray J.D.: Models of epidermal wound healing. Proc. Roy. Soc. London, Ser. B **241** 29 – 36 (1990)
29. Sherratt J. A.: Chemotaxis and chemokinesis in eukaryotic cells: the Keller-Segel equations as an approximation to a detailed model. Bull. Math. Biol. **56** 129 – 146 (1994)
30. Skeel R. D. and Berzins M., A Method for the Spatial Discretization of Parabolic Equations in One Space Variable, SIAM Journal on Scientific and Statistical Computing, **11** 1 – 32 (1990)
31. Stokes C. L. and Lauffenburger D.: Analysis of the roles of microvessel endothelial cell random motility and chemotaxis in angiogenesis. J. Theor. Biol. **152** 377 – 403 (1991)
32. Skowyra D., Georgopoulos C. and Żylicz M.: The E. coli dnaK gene product, the hsp70 homolog, can reactivate heat-inactivated RNA polymerase in an ATP hydrolysis-dependent manner. Cell **62** 939 – 944 (1990)
33. Wickner S., Maurizi M.R., Gottesman S.: Posttranslational Quality Control: Folding, Refolding, and Degrading Proteins. Science **286** 1888 – 1893 (1999)
34. Żylicz M., King F.W. and Wawrzynow A.: Hsp70 interactions with the p53 tumour suppressor protein. EMBO J. **20** 4634 – 4638 (2001)